Pergamon

Int. J. Solids Structures Vol. 34, No. 12, pp. 1479–1491, 1997

0020–7683/97 $17.00 + .00

PII: S0020–7683(96)00099–6

ELASTIC-CRACKED MODEL FOR PENETRATION INTO UNREINFORCED CONCRETE TARGETS WITH OGIVAL NOSE PROJECTILES

Y. XU, L. M. KEER
Northwestern University, Department of Civil Engineering, Technological Institute, 2145 Sheridan Road, Evanston, IL 60208-3109, U.S.A.

and

V. K. LUK
Sandia National Laboratories, PO Box 5800, Albuquerque, NM 87185-0744, U.S.A.

(*Received* 17 *April* 1995; *in revised form* 23 *May* 1996)

Abstract—In this research an elastic-cracked model for determining the forces on an ogival nose projectile is developed to estimate the resistance to penetration into an unreinforced concrete target. The model developed is guided by the post-test observation that concrete will crack in the region surrounding the projectile. In this model the spherical cavity expansion approximation is extended by assuming a cracked region and an elastic region to simulate penetration into an unreinforced concrete target. Thus, an elastic-cracked model is developed here for predicting the resistance to penetration, where it is assumed that the interface of the cracked region and elastic region, which satisfies the Hugoniot jump conditions, is controlled by the radial compressive strength p_0. Solutions that determine the boundary for the elastic region for both incompressible and compressible cases are given. A calculation shows that the incompressible solution is of first-order for the compressive solution when Poisson's ratio equals 0.5. The resistance to penetration depends on the following factors of the concrete target: Poisson's ratio ν, locked volumetric strain η^*, strength of the material and velocity V. The present model predictions of depth of penetration appear to be in good agreement with existing experimental measurements that involve a steel projectile penetrating a thick, unreinforced concrete slab at normal incidence.

1. INTRODUCTION

High-velocity penetration or perforation of geological targets by a projectile is of concern to both military and civilian technology. Studies of high velocity penetration, which began with the pioneering work of Bishop *et al.* (1945), have been applied to the fields of soil mechanics, rock mechanics and impact mechanics. During the past two decades, enormous strides have been made toward understanding the mechanisms involved in the penetration process, which have led to significant improvements in the prediction of these phenomena. Forrestal *et al.* (1981) studied the deep penetration of a projectile, focusing on the depth of penetration, penetrator deceleration history and distribution of stress on the projectile nose. Analytical solutions were given by Forrestal *et al.* (1988) for penetration into an elastic–perfectly plastic target by rigid, long rods having spherical, ogival and conical nose shapes. Using the cavity expansion method and assuming a model having elastic and plastic regions, an analytical evaluation to predict resistance to penetration was given by Luk and Forrestal (1987) in the form, $A + BV^2$, where V is the penetrator velocity and A and B are parameters depending on the material properties of the target and projectile geometry. Later, Luk *et al.* (1991), in a study of elastoplastic materials with power-law strain-hardening, determined the resistance to penetration for strain-hardening materials.

The simulation of the response behavior of a concrete target, when impacted by a projectile, is a very complicated problem. Luk and Forrestal (1987, 1989) used an elastic–plastic model to represent the concrete target response and succeeded in developing an engineering solution for the prediction of the penetration depth. This modeling approach

works reasonably well for heavily reinforced concrete targets. However, this model may only have limited applications for unreinforced concrete targets that behave like brittle materials, where post-test target observation indicates that radial cracks develop in the concrete region surrounding the projectile.

For unreinforced concrete targets, a cracked-elastic model will be assumed to represent the responses of a target when impacted by a projectile. This model is developed here for predicting resistance, where it is assumed that the microcracks that start to develop are controlled by the radial compressive strength p_0 and that the interface between the cracked and elastic regions is connected through Hugoniot jump conditions. The results agree qualitatively with the experimental data and empirical results (Canfield & Clator, 1966; Forrestal *et al.*, 1994).

2. RESISTANCE EVALUATION FOR PENETRATION

The resistance to penetration, on a rigid projectile with an ogival nose shape hitting a target with a velocity V, can be determined from the distribution of the normal stress σ_n around the projectile nose. The distribution of the stress depends on the material properties and the geometry of the target as well as the projectile's velocity.

The resistance to penetration on a projectile with an ogival nose (Luk & Forrestal, 1987) can be written as

$$F_z = 2\pi s^2 \int_{\phi_0}^{\pi/2} \sigma_n [\sin\phi - \sin\phi_0] \cos\phi \, d\phi \tag{1}$$

where $\sin\phi_0 = (s-a)/s$ and the caliber-radius-head (CRH) $\psi = s/2a$ is usually used to describe the nose shape of the penetrator (Fig. 1). Using the dynamic cavity expansion method, the normal stress σ_n, which depends on the transient velocity of the projectile and the material properties of the target, has been estimated by Luk and Forrestal (1987) as

$$\sigma_n = f(A + BV^2 \cos^2\phi) \tag{2}$$

where A and B are parameters depending on the material properties of target, V is the projectile velocity and f is the target yield strength Y for the elastic–plastic model as used by Luk and Forrestal (1987). From (2) the resistance can be written as

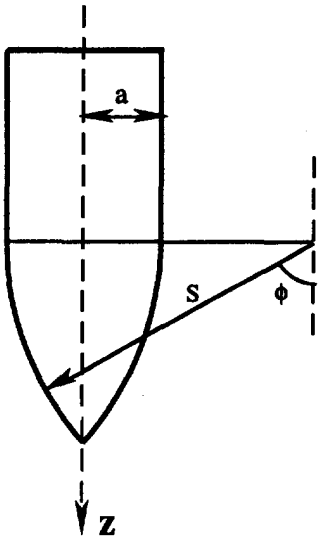

Fig. 1. Geometry of an ogival nose projectile.

$$F_z = \pi a^2 f\left[A + \frac{8\psi - 1}{24\psi^2} BV^2\right] \tag{3}$$

In the present case, the target radial compressive strength p_0 is used for the elastic-cracked model to describe the cracking failure mode. The reason for using the compressive strength p_0 in the cavity expansion model is that brittle materials are subjected to compression in the radial direction and tension in the circumferential direction owing to the cavity expansion force. Concrete under such a complex stress state is assumed to initiate cracking once the stress achieves a certain threshold value. The general criterion of this cracking failure depends on invariants, J_1 and J_2. In the dynamic cavity expansion model, the value of J_1 is nearly zero. Thus, the value of J_2 might be the controlling parameter for the cracked and elastic regions. For convenience as an approximation, the critical compressive stress p_0 is used to distinguish the cracked region and the elastic region. A new set of coefficients A_1 and B_1 is used for this purpose and the computation giving A_1 and B_1 will be derived subsequently.

Equation (3) was derived on the assumption of a region of plastic deformation around the projectile nose and one of elastic deformation outside of the plastic region. Instead of a plastic region, the concept of a "cracked region" is used. This is defined as a region where the hoop stress vanishes when the critical stress is exceeded.

3. CRACKED REGION ANALYSIS FOR DYNAMIC CAVITY EXPANSION

The resistance to penetration on a rigid projectile with an ogival nose shape that hits a target with velocity V has been evaluated by Luk and Forrestal (1987) using an elasto-plastic model in which the spherical cavity expansion approximation by Hopkins (1960) is employed. As shown in Fig. 2, a spherically symmetric cavity expands from zero initial radius at a constant velocity V. When the velocity is sufficiently high, the target material is represented by a locked hydrostat with a constant shear strength. A brittle material generally will not form a plastic region around the projectile, instead, a cracked region may surround the penetrator. Thus, a cavity expansion approximation with elastic and cracked regions is proposed to estimate approximately the resistance of a concrete target to the projectile.

As shown in Fig. 2, the cracked region is bounded by the radii $r = Vt$ and $r = ct$, where c is the velocity of the elastic-cracked boundary, r is the radial Lagrangian coordinate and t is time. According to Hightower (1983), the volumetric strain for the four month concrete under investigation is nearly linear to about 300 MPa and then proceeds to stiffen.

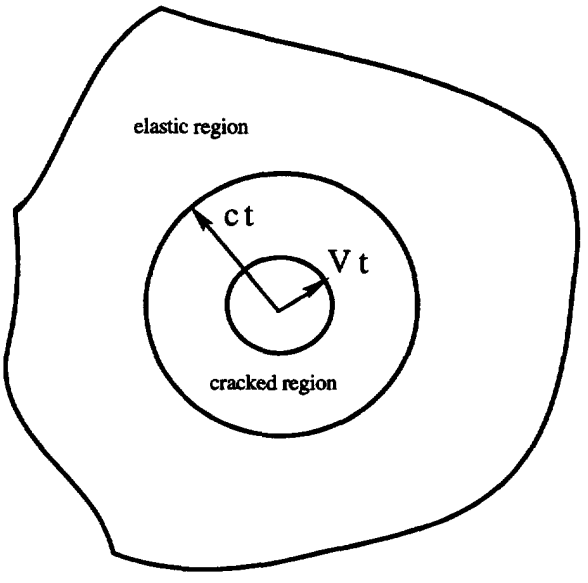

Fig. 2. Response regions for the spherically symmetric cavity expansion.

As an approximation, linear and locked hydrostats have been assumed. For a locked hydrostat in the cracked region,

$$\eta^* = 1-\rho_0/\rho^* \tag{4}$$

where ρ_0 and ρ^* are the initial and locked densities and η^* is the locked volumetric strain. Since the stress distribution arising from the cavity expansion analysis is relatively simple, it is possible to use a radial compressive strength p_0 to determine the boundary between the cracked region and the elastic region. In the cracked region the tensile stress in the circumferential direction will be set to zero. The circumferential stress change from the cracked region to the elastic region is not continuous.

The equations of momentum and mass conservation using Lagrangian coordinates for large deformation are given as

$$(r+u)^2\frac{\partial\sigma_r}{\partial r}+2\left(1+\frac{\partial u}{\partial r}\right)(r+u)(\sigma_r-\sigma_\theta)+\rho_0 r^2\frac{\partial^2 u}{\partial t^2}=0 \tag{5}$$

$$\frac{1}{3}\frac{\partial}{\partial r}[(r+u)^3]=\frac{\rho_0}{\rho}r^2 \tag{6}$$

where r is the Lagrangian coordinate, u is radial displacement (positive outward) and ρ is current density. The normal stress on the projectile nose is approximated by results from the spherical symmetric cavity expansion analysis that relates the cavity expansion velocity to the radial stress σ_r on the cavity surface. For the elastic-cracked model, the hoop stress σ_θ is assumed to vanish in the cracked region. The boundary condition at the cavity surface is

$$u(r,t)|_{r=0}=Vt. \tag{7}$$

It is convenient to introduce the similarity transformation and dimensionless variables as

$$\xi=r/ct,\quad u(r,t)=ct\bar{u}(\xi),\quad S=\sigma_r/p_0. \tag{8}$$

Equation (5) becomes

$$(\xi+\bar{u})^2\frac{\mathrm{d}S}{\mathrm{d}\xi}+2S(\xi+\bar{u})\frac{\mathrm{d}}{\mathrm{d}\xi}(\xi+\bar{u})+\frac{\rho_0\xi^4c^2}{P_0}\frac{\mathrm{d}^2\bar{u}}{\mathrm{d}\xi^2}=0. \tag{9}$$

Since the mass is conserved

$$\frac{1}{3}\frac{\mathrm{d}}{\mathrm{d}\xi}[(\xi+\bar{u})^3]=(1-\eta^*)\xi^2 \tag{10}$$

and

$$\begin{aligned}\frac{\mathrm{d}\bar{u}}{\mathrm{d}\xi}&=\frac{(1-\eta^*)\xi^2}{(\xi+\bar{u})^2}-1\\ \frac{\mathrm{d}^2\bar{u}}{\mathrm{d}\xi^2}&=\frac{2(1-\eta^*)\xi}{(\xi+\bar{u})^2}-\frac{2(1-\eta^*)^2\xi^4}{(\xi+\bar{u})^5}.\end{aligned} \tag{11}$$

The solution to (9) is

$$S = \frac{-\rho_0 c^2}{p_0(\xi+\bar{u})^2}\int\left\{\frac{2(1-\eta^*)\xi^5}{(\xi+\bar{u})^2} - \frac{2(1-\eta^*)^2\xi^8}{(\xi+\bar{u})^5}\right\}d\xi + \frac{D}{(\xi+\bar{u})^2} \tag{12}$$

where the constant D is to be determined from the boundary condition at the elastic-cracked interface. The boundary condition

$$\bar{u}|_{\xi=0} = V/c \tag{13}$$

allows (10) to be written as

$$(\xi+\bar{u})^3 = (1-\eta^*)\xi^3 + (V/c)^3. \tag{14}$$

Substitution of (14) into (12) yields

$$S = \frac{-\rho_0 c^2}{p_0[(1-\eta^*)\xi^3+(V/c)^3]^{2/3}}\int\frac{2(1-\eta^*)(V/c)^3\xi^5}{[(1-\eta^*)\xi^3+(V/c)^3]^{5/3}}d\xi + \frac{D}{[(1-\eta^*)\xi^3+(V/c)^3]^{2/3}}. \tag{15}$$

The integral of (15) can be calculated to yield

$$S = \frac{-\rho_0 c^2(V/c)^3}{p_0(1-\eta^*)[(1-\eta^*)\xi^3+(V/c)^3]^{4/3}}\{2(1-\eta^*)\xi^3+3(V/c)^3\} + \frac{D}{[(1-\eta^*)\xi^3+(V/c)^3]^{2/3}}. \tag{16}$$

The constant D can be determined by the boundary condition $S = S_2$ when $\xi = 1$. Thus S can be written as

$$S(\xi) = \frac{\rho_0 c^2(V/c)^3}{p_0(1-\eta^*)[(1-\eta^*)\xi^3+(V/c)^3]^{2/3}}\left\{\frac{2(1-\eta^*)+3(V/c)^3}{[(1-\eta^*)+(V/c)^3]^{2/3}} - \frac{2(1-\eta^*)\xi^3+3(V/c)^3}{[(1-\eta^*)\xi^3+(V/c)^3]^{2/3}}\right\} + S_2\frac{[(1-\eta^*)+(V/c)^3]^{2/3}}{[(1-\eta^*)\xi^3+(V/c)^3]^{2/3}}. \tag{17}$$

The analysis of elastic region will determine the radial stress S_2 in (17).

4. STRESS ANALYSIS FOR COMPRESSIBLE ELASTIC REGION

The elastic response for a compressible material is governed by the equation

$$\frac{\partial\sigma_r}{\partial r} + \frac{2(\sigma_r-\sigma_\theta)}{r} = -\rho\frac{\partial^2 u}{\partial t^2}. \tag{18}$$

Here the negative term on the right side of (18) is due to the definition of compressible stress as positive. The stress-displacement relations

$$\sigma_r = -\frac{E}{(1+\nu)(1-2\nu)}\left[(1-\nu)\frac{\partial u}{\partial r} + 2\nu\frac{u}{r}\right]$$

$$\sigma_\theta = -\frac{E}{(1+\nu)(1-2\nu)}\left[\nu\frac{\partial u}{\partial r} + \frac{u}{r}\right] \tag{19}$$

result in the governing equation (18) as

$$\frac{\partial^2 u}{\partial r^2}+\frac{2}{r}\frac{\partial u}{\partial r}-\frac{2u}{r^2}=\frac{1}{c_1^2}\frac{\partial^2 u}{\partial t^2} \tag{20}$$

where c_1 is the longitudinal wave speed as

$$c_1=\sqrt{\frac{E(1-v)}{\rho(1+v)(1-2v)}} \tag{21}$$

and E is Young's modulus and v is Poisson's ratio. The substitution of dimensionless displacement in (8) into (20) gives

$$(1-\alpha^2\xi^2)\frac{\mathrm{d}^2\bar{u}}{\mathrm{d}\xi^2}+\frac{2}{\xi}\frac{\mathrm{d}\bar{u}}{\mathrm{d}\xi}-\frac{2}{\xi^2}\bar{u}=0 \tag{22}$$

where $\alpha=c/c_1$ and the solution to (22) is

$$\bar{u}=A_{\mathrm{D}}\alpha\xi-B_{\mathrm{D}}\left(\frac{1-3\alpha^2\xi^2}{3\alpha^2\xi^2}\right) \tag{23}$$

where the coefficients A_{D} and B_{D} can be determined by the conditions of zero displacement at the elastic wave front and the stress jump on the elastic-cracked interface, i.e.

$$\bar{u}|_{\xi=1/\alpha}=0,\quad \alpha_r|_{\xi=1}=p_0. \tag{24a,b}$$

Here (24a) indicates that the displacement at the wave front is zero and (24b) shows that the compressive stress at the interface of the cracked region and elastic region is p_0. Therefore, the displacement in (23) can be written as

$$\bar{u}(\xi)=\frac{p_0}{2E}K(v,\alpha)\left[2\alpha^3\xi+\frac{1-3\alpha^2\xi^2}{\xi^2}\right] \tag{25}$$

where

$$K(v,\alpha)=\frac{(1+v)(1-2v)}{3v\alpha^3-(1+v)\alpha+(1-2v)}. \tag{26}$$

If it is assumed that $\alpha \ll 1$, then the first-order solution of the displacement and stresses is

$$\bar{u}(\xi)=\frac{p_0}{2E}\frac{1+v}{\xi^2},\sigma_r=\frac{p_0}{\xi^3},\quad \sigma_\theta=-\frac{p_0}{2\xi^3}, \tag{27}$$

and for $v=\frac{1}{2}$, (27) is reduced to the incompressible elastic solution.

Since

$$\sigma_r-\sigma_\theta=-\frac{3p_0}{2(1+v)}K(v,\alpha)\left[\frac{\alpha^2}{\xi}-\frac{1}{\xi^3}\right] \tag{28}$$

equation (18) can be written as

$$\frac{dS}{d\xi} = \frac{3}{1+\nu}K(\nu,\alpha)\left[\frac{\alpha^2}{\xi^2} - \frac{1}{\xi^4}\right] - 3\rho c^2 K(\nu,\alpha)\frac{1}{E\xi^2}. \tag{29}$$

Thus

$$S(\xi) = \frac{3}{1+\nu}K(\nu,\alpha)\left[-\frac{\alpha^2}{\xi} + \frac{1}{3}\frac{1}{\xi^3}\right] + 3\rho c^2 K(\nu,\alpha)\frac{1}{E\xi}. \tag{30}$$

To the first-order solution of the stress, $S(\xi)$ is

$$S(\xi) = \frac{1}{\xi^3} + \frac{3(1+\nu)\rho c^2}{E\xi}. \tag{31}$$

For $\nu = 1/2$, this stress is the same as the incompressible elastic solution. Here the radial stress $S(\xi)$ and the interface velocity c will be used to derive the resistance to penetration on the projectile in terms of interface conditions. If V is the particle velocity and its dimensionless form is defined as $U = v/c$, then the first-order elastic compressible solutions can be reduced to

$$\begin{aligned} \bar{u}(\xi) &= \frac{p_0}{2E}\frac{1+\nu}{\xi^2} \\ U(\xi) &= \frac{3p_0}{2E}\frac{1+\nu}{\xi^2} \\ S(\xi) &= \frac{1}{\xi^3} + \frac{3(1+\nu)\rho c^2}{E\xi}. \end{aligned} \tag{32}$$

The resistance to penetration on a penetrator can be evaluated using (17) and (32) in terms of interface conditions.

5. RESISTANCE FORMULA FOR ELASTIC-CRACKED MODEL

In the penetration model it is, in general, assumed that the Hugoniot jump conditions are satisfied across the interface of two regions. Here the cracked and the elastic regions are connected through the Hugoniot jump conditions that conserve mass and momentum across the interface (Luk & Forrestal, 1987),

$$\begin{aligned} \rho_2(v_2 - c) &= \rho_1(v_1 - c) \\ \sigma_2 + \rho_2 v_2(v_2 - c) &= \sigma_1 + \rho_1 v_1(v_1 - c) \end{aligned} \tag{33}$$

where the subscripts 2 and 1 refer, respectively, to quantities at the elastic-cracked interface ($\xi = 1$) in the cracked and elastic regions. For a locked hydrostat in the cracked region and a compressible material in the elastic region, $\rho_2 = \rho^*$ and $\rho_1 = \rho$ and the dimensionless jump conditions can be expressed as

$$\begin{aligned} U_2 &= 1 - \frac{\rho}{\rho_0}(1-\eta^*)(1-U_1) \\ S_2 &= S_1 + \frac{\rho c^2}{p_0}(1-U_1)^2\left[1 - \frac{\rho}{\rho_0}(1-\eta^*)\right]. \end{aligned} \tag{34}$$

Equation (34) combined with the analysis of cracked region and elastic region will give the resistance formula for penetration.

For a compressible elastic region, the first-order solution is expressed in (32). At the interface between the elastic and the cracked regions where $\xi = 1$,

$$\bar{u}_1 = (1+\nu)\frac{p_0}{2E}$$

$$U_1 = 3(1+\nu)\frac{p_0}{2E}$$

$$S_1 = 1+3(1+\nu)\frac{\rho c^2}{E} \tag{35}$$

and from (14), the interface velocity is $c = V\gamma^{-1}$, where

$$\gamma = \left\{\left[1+(1+\nu)\frac{p_0}{2E}\right]^3 - (1-\eta^*)\right\}^{1/3}. \tag{36}$$

Substitution of (35) into (34) gives

$$S_2 = 1+\frac{\rho c^2}{p_0}\left\{3(1+\nu)\frac{p_0}{E} + \left[1-3(1+\nu)\frac{p_0}{2E}\right]^2\left[1-\frac{\rho}{\rho_0}(1-\eta^*)\right]\right\}. \tag{37}$$

With the aid of (17), the radial stress in the cracked region can be written as

$$S(\xi) = \frac{\rho_0 V^2\gamma}{p_0(1-\eta^*)[(1-\eta^*)\xi^3+\gamma^3]^{2/3}}\left\{\frac{2(1-\eta^*)+3\gamma^3}{[(1-\eta^*)+\gamma^3]^{2/3}} - \frac{2(1-\eta^*)\xi^3+3\gamma^3}{[(1-\eta^*)\xi^3+\gamma^3]^{2/3}}\right\}$$
$$+\frac{[(1-\eta^*)+\gamma^3]^{2/3}}{[(1-\eta^*)\xi^3+\gamma^3]^{2/3}}\left\{1+3(1+\nu)\frac{\rho V^2}{E\gamma^2}+\frac{\rho V^2}{p_0\gamma^2}\left[1-3(1+\nu)\frac{p_0}{2E}\right]^2\left[1-\frac{\rho}{\rho_0}(1-\eta^*)\right]\right\}. \tag{38}$$

The radial stress at the cavity surface where $\xi = 0$ is

$$S(0) = A_1 + B_1 V^2$$

where

$$A_1 = \lambda\gamma^{-2}$$

$$B_1 = \frac{\rho_0}{p_0(1-\eta^*)}\left[\frac{2(1-\eta^*)+3\gamma^3}{\lambda\gamma} - 3\right]$$
$$+\frac{\rho\lambda}{p_0\gamma^4}\left\{3(1+\nu)\frac{p_0}{E}+\left[1-3(1+\nu)\frac{p_0}{2E}\right]^2\left[1-\frac{\rho}{\rho_0}(1-\eta^*)\right]\right\}$$

$$\lambda = \left[1+(1+\nu)\frac{p_0}{2E}\right]^2. \tag{39}$$

The material density ρ of the elastic region in (39) can be evaluated in terms of the material deformation on the boundary of the elastic region ($\xi = 1$). If the volume expansion is ΔA,

then the density

$$\rho = \frac{\rho_0}{1+\Delta A} \quad \text{and} \quad \Delta A = \frac{\partial u}{\partial r} + \frac{2u}{r}.$$

The displacement representation (25) gives

$$\frac{\partial u}{\partial r} + \frac{2u}{r} = -\frac{3(1-\alpha)\alpha^2(1+\nu)(1-2\nu)}{3\nu\alpha^3 - (1+\nu)\alpha^2 + (1-2\nu)} \frac{p_0}{E}. \tag{40}$$

Thus, the material density in the elastic region can be written as

$$\rho = \rho_0 \left[1 + \frac{3(1-\alpha)\alpha^2(1+\nu)(1-2\nu)}{3\nu\alpha^3 - (1+\nu)\alpha^2 + (1-2\nu)} \frac{p_0}{E} \right]. \tag{41}$$

It is clear that in the case of either $\nu = 1/2$ or the first-order approximation, the density of the elastic material is $\rho = \rho_0$. Therefore, corresponding coefficients of (39) for the resistance of the first-order approximation with $\nu = 1/2$ are

$$A_1 = \gamma^{-2}\left(1 + \frac{3p_0}{4E}\right)^2 \tag{42}$$

$$B_1 = \frac{\rho_0}{p_0}\left\{ \frac{1}{1-\eta^*}\left[\frac{3\left(1+\frac{3p_0}{4E}\right)^3 - (1-\eta^*)}{\left(1+\frac{3p_0}{4E}\right)^2 \gamma} - 3 \right] + \left(1+\frac{3p_0}{4E}\right)^2 \left[\frac{9p_0}{2E} + \eta^* \left(1 - \frac{9p_0}{4E}\right)^2 \right] \gamma^{-4} \right\} \tag{43}$$

where

$$\gamma = \left[\left(1 + \frac{3p_0}{4E}\right)^3 - (1-\eta^*) \right]^{1/3}. \tag{44}$$

Figure 3 shows the radial stress at the cavity surface vs cavity expansion velocity for

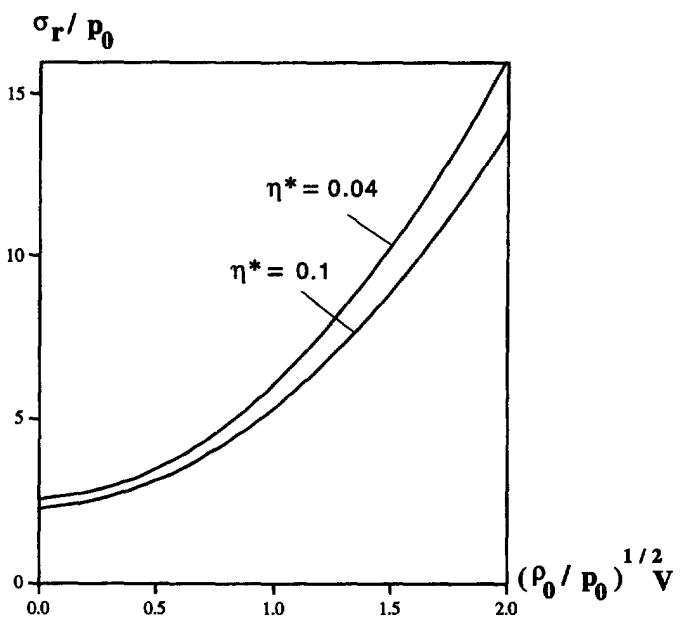

Fig. 3. Radial stress on the cavity surface for an incompressive solution vs cavity expansion velocity.

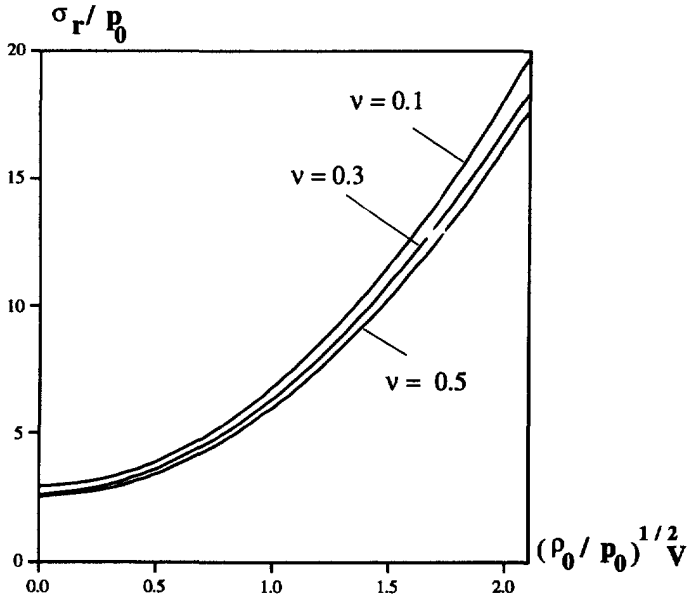

Fig. 4. Radial stress on the cavity surface for a material with $\eta^* = 0.04$ vs cavity expansion velocity.

an incompressible material in the elastic region (i.e. $\nu = 1/2$ and $\rho = \rho_0$) with $\eta^* = 0.04$ and 0.10. Analogous to the elastic–plastic model by Luk and Forrestal (1987), the radial stress has a weak dependence on the locked volumetric strain η^* for the elastic-cracked model. A similar plot of the radial stress at the cavity surface vs cavity expansion velocity is shown in Fig. 4 for a compressible material with $\eta^* = 0.04$ and various Poisson's ratio ν. As indicated in Fig. 4, the radial stress depends weakly on ν.

The calculation of the resistance to penetration by the projectile and the depth of penetration have been studied by Luk and Forrestal (1987). Integration of the radial stress on the projectile nose gives the resistance to penetration by the penetrator,

$$F_z = \alpha_1 + \beta_1 V_z^2 \tag{45}$$

where V_z is the projectile velocity and the coefficients α_1 and β_1 are determined by the properties of the target and the geometry of the projectile as

$$\alpha_1 = \pi a^2 p_0 A_1, \quad \beta_1 = \pi a^2 p_0 B_1 \frac{8\psi - 1}{24\psi^2}. \tag{46}$$

The depth of penetration into a semi-infinite medium is

$$P_t = \frac{m}{2\beta_1} \ln\left(\frac{\alpha_1 + \beta_1 V_0^2}{\alpha_1 + \beta_1 V_t^2}\right) \tag{47a}$$

$$P = \frac{m}{2\beta_1} \ln\left(1 + \frac{\beta_1}{\alpha_1} V_0^2\right) \tag{47b}$$

where m is the mass of the penetrator and P_t is the depth as the velocity of the penetrator decreases from an impact velocity V_0 to the transient velocity V_t. The maximum depth of the penetrator as the projectile stops is P.

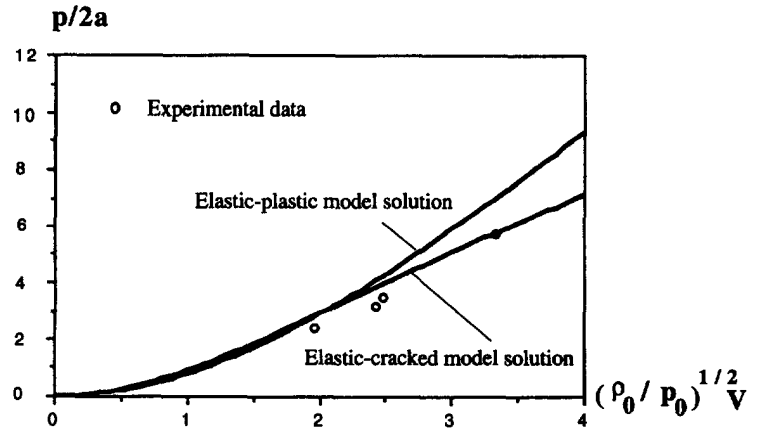

Fig. 5. Comparison of scaled penetration depths from elastic-cracked and elastic-plastic models with experimental data (Canfield & Clator [1966]).

It is informative to compare the predictive performance of the penetration models between the elastic-cracked model described in this paper and the elastic-plastic model developed by Luk and Forrestal (1987). Figure 5 compares the depth of penetration predictions from these two models with the experimental data collected by Canfield and Clator (1966). In their experimental setup, Canfield and Clator used penetrators with an ogival nose of caliber-radius-head, $\psi = 1.5$, diameter of 76.2 mm and mass of 5.9 kg. The density of the concrete target material $\rho_0 = 2240$ kg m^{-3} and $p_0 = 64$ MPa. Figure 5 shows that the depth of penetration predictions from the two models are in very close agreement with each other in the lower velocity range until $(\rho_0/p_0)^{1/2}V = 2.5$, where divergence starts to occur. In addition, the predictions from both models are in reasonably good agreement with the experimental data.

The depth of penetration predictions from the elastic-cracked model is also compared with the experimental data collected by Forrestal *et al.* (1994) in Fig. 6. In this experimental set-up with unreinforced concrete targets, the density of the target material is $\rho_0 = 2370$ kg m^{-3} and $p_0 = 67$ MPa. The diameter of the projectile is 26.9 mm and the mass is 0.906 kg with an ogival nose of caliber-radius-head, $\psi = 2.0$. The plotted results indicate that the model predictions are in good agreement with the experimental data.

The cracks in the elastic-cracked model are controlled by the radial compressive strength p_0. The sensitivity of this material parameter to the depth of penetration is demonstrated in Fig. 7. Curves show two penetration cases with impact velocity of 300 and 500

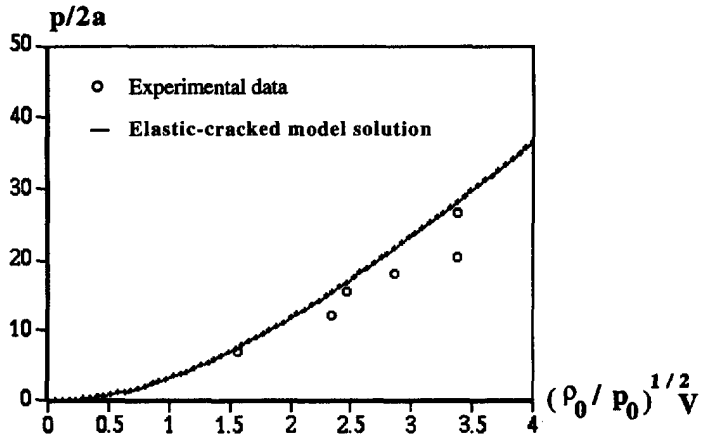

Fig. 6. Comparison of scaled penetration depth from elastic-cracked model with experimental data (Forrestal *et al.* [1994]).

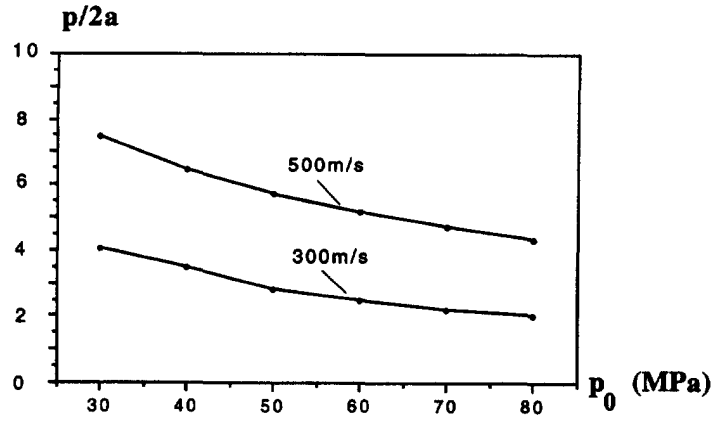

Fig. 7. Scaled penetration depth vs compressive strength p_0.

m s^{-1} for the experimental set-up described in Fig. 5. Results indicate that the penetration depth reduces with increasing radial compressive strength.

6. CONCLUSION

An elastic-cracked model, based on the dynamic spherical cavity expansion method, has been applied to simulate approximately the penetration of a projectile into an unreinforced concrete target and to develop an engineering solution for estimating forces on projectiles and penetration depths. For an ogival nose projectile penetrating into unreinforced concrete targets, the interface between the cracked and the elastic regions satisfies the Hugoniot jump conditions that conserve mass and momentum across the interface. Calculations show that a solution based on the incompressible assumption is a special solution of the first-order compressible solutions when the Poisson's ratio equals 0.5. In addition, the resistance to projectile penetration depends mainly on impact velocity, projectile mass and material properties, such as compressive strength p_0 and elastic modulus E, but depends weakly on Poisson's ratio v and the locked volumetric strain η^*. The penetration depth predicted by the elastic-cracked modes agrees well with the experimental measurements.

It has been demonstrated that the elastic-cracked model produces predictions on penetration depths that are very close to those provided by the elastic-plastic model developed by Luk and Forrestal (1987). The two models are used to provide an approximate simulation of two different material responses in concrete targets, depending on the amount of reinforcement in them. For unreinforced concrete targets impacted by a projectile, cracks will be initiated and propagated in the region close to the projectile. Quite appropriately, the elastic-cracked model should be used to simulate the concrete target responses. On the other hand, the elastic–plastic model is the appropriate choice for heavily reinforced concrete targets where most cracks are arrested by the closely spaced reinforcing bars.

The elastic-cracked model provides an approximate method to deal with the damage region in the concrete target close to the projectile. Therefore this method may offer a useful tool for research efforts to simulate the cracking mechanisms of concrete target responses that are associated with the perforation of thin concrete targets.

Acknowledgement—The research conducted by Doctors Y. Xu and L. M. Keer at Northwestern University was supported by a contract PR no. AF-6802, from Sandia National Laboratories. The work by Dr V. K. Luk was performed at Sandia National Laboratories, which is operated for the U.S. Department of Energy under contract DE-AC04-94AL85000.

REFERENCES

Bishop, R. F., Hill, R. and Mott, N. F. (1945) The theory of indentation and hardness tests. *Proceedings of the Physics Society* **57**, 147–159.

Canfield, J. A. and Clator, I. G. (1966) Development of a scaling law and techniques to investigate penetration in concrete. In *NWL Report* no. 2057. U.S. Naval Weapons Laboratory, Dahlgren, VA.

Forrestal, M. J., Norwood, F. R. and Longcope, D. B. (1981) Penetration into targets described by locked hydrostats and shear strength. *Journal of Applied Mechanics* **55,** 275–279.

Forrestal, M. J., Okajima, K. and Luk, V. K. (1988) Penetration of 6061-T651 aluminum targets with rigid long rods. *Journal of Applied Mechanics* **55,** 755–760.

Forrestal, M. J., Altman, B. S., Cargile, J. D. and Hanchak, S. J. (1994) An empirical equation for penetration depth of ogival-nose projectile into concrete targets. *International Journal of Impact Engineering* **15,** 395–405.

Hightower, M. M. (1983) The effects of curing and aging on the triaxial properties of concrete in underground structure. In *Symp. Proc. for the Interaction of Non-Nuclear Munitions with Structures*, pp. 65–68. U.S. Air Force Academy, CO.

Hopkins, H. G. (1960) Dynamic expansion of spherical cavities in metals. *Progress in Solid Mechanics*, Vol. 1 (eds I. N. Sneddon and R. Hill). North-Holland Publishing Co., Amsterdam.

Luk, V. K. and Forrestal, M. J. (1987) Penetration into semi-infinite reinforced concrete targets with spherical and ogival nose projectiles. *International Journal of Impact Engineering* **6**(4), 291–301.

Luk, V. K. and Forrestal, M. J. (1989) Comment on penetration into semi-infinite reinforced concrete targets with spherical and ogival nose projectiles. *International Journal of Impact Engineering* **8**(1), 83–84.

Luk, V. K., Forrestal, M. J. and Amos, D. E. (1991) Dynamic spherical cavity expansion of strain-harding materials. *Journal of Applied Mechanics* **58,** 1–6.